Editors' Suggestion

Reduced finite-dimensional model of two-dimensional protein cluster formation

Kevin Chen and Paul C. Bressloff
Department of Mathematics, Imperial College London, London SW7 2AZ, United Kingdom

(Received 12 May 2026; accepted 24 July 2026; published 8 September 2026)

The aggregation or clustering of proteins plays an important role in the formation of postsynaptic domains (PSDs) at excitatory and inhibitory synapses in neurons. PSDs are rich in scaffolding proteins that can transiently trap transmembrane neurotransmitter receptors, allowing them to regulate the strength of synaptic connections during learning and memory. Recently, a two-dimensional diffusion-mediated aggregation model of PSD formation was developed in which the spatial locations of the clusters are determined by a set of fixed anchoring sites. The system is kept out of equilibrium by the recycling of particles between the cell membrane and interior. This results in a nontrivial stationary state consisting of multiple stable protein clusters. In this paper, we use matched asymptotic methods to reduce the underlying reaction-diffusion model with moving interior boundaries to a corresponding finite-dimensional nonlinear system. The latter couples the cluster radii to the spatially averaged protein concentration in the bulk domain. We assume that the diffusivity D is $O(1/\nu)$, where $\nu = -1/\ln\epsilon$ and ϵ is a small parameter that characterizes the size of the clusters relative to the size of the bulk domain. The reduced dynamical system allows us to explore both the existence and stability of the multicluster stationary state while maintaining the effects of diffusion-mediated interactions between clusters.

DOI: 10.1103/j7dy-7djl

I. INTRODUCTION

An important mechanism for enhancing the effective strength of synaptic connections between neurons is the transient trapping of protein receptors within postsynaptic domains (PSDs) that are directly aligned with the presynaptic active zones for neurotransmitter release [1–5]. Each PSD is rich in scaffolding proteins that dynamically form clusters via a combination of lateral membrane diffusion and the recycling of proteins between the cell surface and interior. Recently, a two-dimensional (2D) diffusion-mediated aggregation and recycling model of PSD formation has been developed in which the clusters are anchored at fixed adhesion sites [6,7]. The anchored clusters were taken to be circular discs with absorbing interfaces whose time-dependent radii were determined by the interplay between the particle fluxes at the interfaces and recycling currents. (Including the aggregation of different-sized diffusing clusters away from anchoring sites would require solving more complicated Smoluchowski coagulation equations [8,9].) The corresponding reaction-diffusion equations were shown to support a nonequilibrium stationary state whose average cluster size was determined using an effective mean-field description of the steady-state particle concentration around each anchored cluster [6]. Extensive numerical simulations established that the stationary clusters are stable [6]. Moreover, corrections to the mean-field approximation were obtained by applying the theory of steady-state diffusion in singularly perturbed domains [7]. The latter involved matching an inner solution around each individual cluster to an outer solution in the bulk domain, resulting in $O(\nu)$ corrections to mean field theory, where $\nu = -1/\ln\epsilon$ and ϵ is the characteristic size of a cluster [7].

In our previous work, we assumed that (i) the particle density within a cluster is much higher than the bulk domain and (ii) the diffusivity $D = O(1)$. Recently, we investigated what can happen if assumption (i) breaks down by considering the simpler case of a one-dimensional (1D) model. We treated the formation of a cluster as a moving boundary problem [10]. This allowed us to adapt spectral and numerical methods previously developed in a study of of tubulin-based neurite elongation, in which the tip of the neurite is treated as a moving boundary subject to polymerization or depolymeriztion [11,12]. We showed that, as expected, a high density cluster in a sea of low density diffusing proteins is always linearly stable. On the other hand, a low density cluster can become unstable via a Hopf-like oscillatory instability resulting in bounded oscillations of the cluster size. These results extended to a 2D cluster.

In this paper, we investigate protein aggregation dynamics in the fast diffusion regime $D = O(\nu^{-1})$ for which assumption (ii) no longer holds. We proceed by making a formal analogy between the diffusion-mediated protein aggregation model and a previous model of diffusion-mediated quorum sensing (QS) [13–15]. In the latter case, the localized compartments represent bacterial cells of fixed size that secrete signaling molecules known as autoinducers into the intercellular space. The resulting buildup of extracellular autoinducer concentration then provides a feedback signal that depends on the cell density. Once the cell density reaches a critical level, the global feedback activates signaling pathways within

the cells that results in some form of coordinated behavior. Matched asymptotics in the fast diffusion limit can be used to reduce the infinite-dimensional system of partial differential equations (PDEs) to an effective finite-dimensional system of nonlinear ordinary differential equations (ODEs) that couple the internal reaction kinetics within each cell to the spatially averaged extracellular autoinducer concentration [15]. The reduced system establishes the emergence and synchronization of oscillatory intracellular dynamics that is mediated by bulk diffusion. Following along analogous lines to Ref. [15], we use matched asymptotic methods to reduce the full protein aggregation-removal model to a corresponding nonlinear ODE model. The latter couples the spatially averaged protein concentration in the bulk domain to the dynamically varying cluster radii. The reduced dynamical system thus allows us to explore both the existence and stability of the multicluster stationary state. We show that the basic qualitative dynamics is captured at $O(1)$ with respect to the asymptotic expansion in ν. In particular, the stationary state lies within a two-dimensional invariant manifold to which the system converges. We analyze the associated planar dynamics and determine the rate of convergence to the invariant manifold. We also explore the effects of higher-order corrections by considering the example of a pair of clusters in the unit disk.

Although the long-term dynamics of the protein aggregation model is simple from a dynamical systems perspective, identifying mechanisms that support that coexistence of multiple membraneless regions of high protein concentration within cells has emerged as a major topic in theoretical biophysics. In particular, there is considerable current interest in so-called biological condensates that arise via a nonequilibrium generalization of liquid-liquid phase separation via Ostwald ripening [16–20]. In many cases, the persistence of multiple condensates is driven by active biochemical reactions within the cell. Such active processes are needed to counteract classical Oswtald ripening in which smaller clusters shrink at the expense of the growth of larger clusters ultimately resulting in a single high-density droplet. As highlighted in Ref. [9], one characteristic feature of active phase separation is that the growth of the condensed phase is limited by the depletion of the dilute phase and thus depends on the size of the bulk domain (whole cell, cell nucleus, dendritic spine). On the other hand, the nonequilibrium stationary state of the protein aggregation and recycling model allows the formation of multiple localized clusters of definite size, such as PSDs, irrespective of the size of the domain in which they form.

II. AGGREGATION-REMOVAL MODEL OF PROTEIN CLUSTERING

Suppose that at time t, $t \geqslant 0$, a 2D bounded domain $\Omega \subset \mathbb{R}^2$ contains a set of N circularly symmetric PSD clusters represented by the subdomains $\mathcal{U}_j(t) \subset \Omega$, $j = 1, \ldots, N$, with radii $R_j(t)$ and centers fixed at the anchoring sites $\mathbf{x}_j \in \Omega$; see Fig. 1. That is,

$$\mathcal{U}_j(t) = \{\mathbf{x} \in \Omega,\ |\mathbf{x} - \mathbf{x}_j| \leqslant R_j(t)\}. \tag{2.1}$$

We assume that scaffolding proteins can freely diffuse in the domain $\Omega\backslash\mathcal{U}(t)$ for $\mathcal{U}(t) = \cup_{j=1}^{N}\mathcal{U}_j(t)$, whereas particles within each cluster efficiently rearrange themselves to

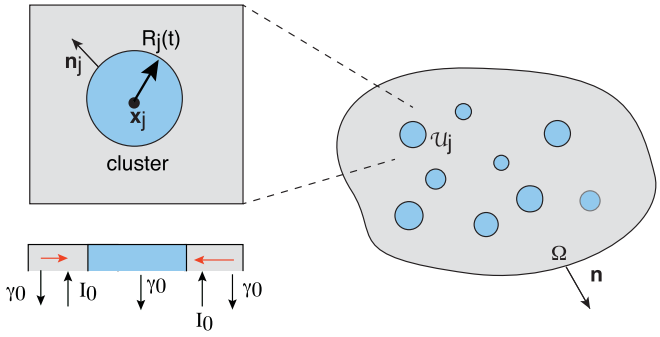

FIG. 1. 2D model of diffusion-based protein cluster formation in the presence of anchoring sites and particle recycling. Particles diffuse in a bounded domain Ω containing N clusters $\mathcal{U}_j$ centered at $\mathbf{x}_j$, $j = 1, \ldots, N$. The cluster radius of the ith cluster at time t is $R_j(t)$. The clusters are dynamically maintained by a combination of lateral diffusion outside the clusters and particle recycling.

maintain a uniform concentration u_0. This means that the total number of proteins within the jth cluster at time t is $\mathcal{N}_j(t) = |\mathcal{U}_j(t)|u_0$, where $|\mathcal{U}_j(t)| = \pi R_j^2(t)$ is the area of the cluster. Motivated by experimental studies of PSD formation at inhibitory synapses [3–5,9], we assume that there is a constant turnover of proteins via exoocytosis or endocytosis. That is, both freely diffusing proteins and proteins within the cluster can be removed at a rate γ_0 (endocytosis) and injected outside the cluster from intracellular pools at a constant flux I_0 (exocytosis). Let $c(\mathbf{x}, t)$ denote the concentration of freely diffusing particles (monomers), which evolves according to the diffusion equation

$$\frac{\partial c(\mathbf{x}, t)}{\partial t} = D\nabla^2 c(\mathbf{x}, t) - \gamma_0 c(\mathbf{x}, t) + I_0, x \in \Omega\backslash\mathcal{U}(t), \tag{2.2a}$$

$$D\nabla c(\mathbf{x}, t) \cdot \mathbf{n} = 0, \quad \mathbf{x} \in \partial\Omega, \tag{2.2b}$$

$$D\nabla c(\mathbf{x}, t) \cdot \mathbf{n}_j(\mathbf{x}) = \kappa c(\mathbf{x}, t), \quad \mathbf{x} \in \partial\mathcal{U}_j(t). \tag{2.2c}$$

Here $\mathbf{n}$ and $\mathbf{n}_j$ are the outward unit normals to the surfaces $\partial\Omega$ and $\partial\mathcal{U}_j$, respectively, D is the diffusivity, the constant γ_0 denotes the recycling or turnover rate of individual particles outside a cluster, and I_0 is the flux of injected particles from intracellular pools. The exterior boundary $\partial\Omega$ is taken to be totally reflecting, whereas the cluster boundaries are assumed to be partially absorbing with reactivities κ. (In our previous work, we took the interfaces to be totally absorbing [7]. This case is recovered in the limit $\kappa \to \infty$. For simplicity, we take the reactivity to be the same for each cluster. However, one could extend the analysis to the case of heterogeneous reactivities κ_j, $j = 1, \ldots, N$.) Thus, each cluster acts as a sink that grows at a rate that depends on the total influx through the surface $\partial\mathcal{U}_j$. However, this growth is counteracted by the recycling of proteins within $\mathcal{U}_j$. (For concreteness, we assume that the rate of recycling within a cluster is also γ_0 and that no particles are injected directly into the cluster.) From particle conservation, the total number of particles within the jth cluster at time t evolves as

$$\frac{d}{dt}\mathcal{N}_j(t) = D\int_{\partial\mathcal{U}_j(t)} \nabla c(\mathbf{x}, t) \cdot \mathbf{n}_j(\mathbf{x}) d\mathbf{x} - \gamma_0 \mathcal{N}_j(t). \tag{2.3}$$

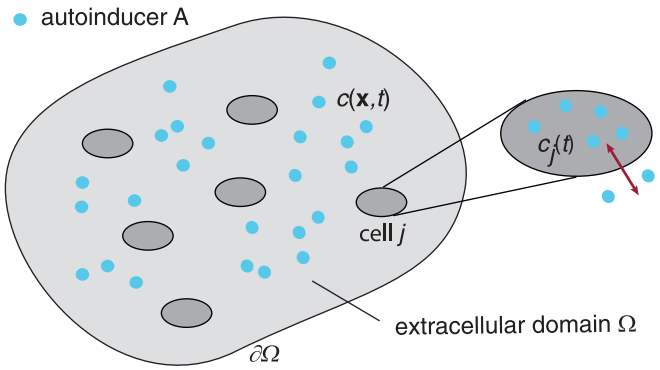

FIG. 2. Schematic diagram showing a population of cells labeled $j = 1, \ldots, N$ that can exchange an autodinducer A with the extracellular domain Ω. The extracellular concentration of A is denoted by $c(\mathbf{x}, t)$ and the intracellular concentration of A in the jth cell is denoted by $c_j(t)$.

Equations (2.2a)–(2.2c) for fixed cluster sizes are formally similar to a nonlinear PDE-ODE model of diffusion-mediated bacterial QS [13–15]. Each subdomain $\mathcal{U}_j$ now has a fixed radius R_j and represents a bacterial cell at a fixed location $\mathbf{x}_j$, whereas $\Omega\backslash\mathcal{U}(t)$ represents the extracellular domain; see Fig. 2. The concentration of extracellular autoinducer $c(\mathbf{x}, t)$ evolves according to the coupled PDE-ODE model

$$\frac{\partial c(\mathbf{x}, t)}{\partial t} = D\nabla^2 c(\mathbf{x}, t) - \gamma_0 c(\mathbf{x}, t), \quad \mathbf{x} \in \Omega\backslash\mathcal{U}, \tag{2.4a}$$

$$D\nabla c(\mathbf{x}, t) \cdot \mathbf{n} = 0, \quad \mathbf{x} \in \partial\Omega, \tag{2.4b}$$

$$D\nabla c(\mathbf{x}, t) \cdot \mathbf{n}_j = \kappa(c(\mathbf{x}, t) - c_j(t)), \quad \mathbf{x} \in \partial\mathcal{U}_j \tag{2.4c}$$

for $j = 1, \ldots, N$, where γ_0 is the rate of particle degradation in the bulk, and u_j is the (uniform) intracellular autoinducer concentration of the jth cell. It is also assumed that there are K other chemical species within each cell, which together with the signaling molecule comprise a regulatory network. Assuming mass action kinetics leads to the following system of equations for the concentrations $\mathbf{w}_j = (w_{j,0}, w_{j,1}, \ldots, w_{j,K})$, where $w_{j,0} \equiv c_j$:

$$\frac{dw_{j,a}}{dt} = f_a(\mathbf{w}_j) - \frac{\kappa\delta_{a,0}}{|\mathcal{U}_j|}\int_{\partial\mathcal{U}_j}(c_j(t) - c(\mathbf{x}, t))d\mathbf{x} \tag{2.5}$$

for $a = 0, 1, \ldots, K$. Here $f_a(\mathbf{w}_j)$ denotes a nonlinear reaction kinetic function. [The factor of $|\mathcal{U}_j|$ ensures that the number of particles crossing $\partial\mathcal{U}_j$ is consistent with the definition of the flux in the boundary condition (2.4c).] One can view Eqs. (2.4) and (2.5) as a nonlinear PDE-ODE model of diffusion-mediated communication between small signaling compartments [13–15].

One common feature of both Eqs. (2.2) and (2.4) is that they involve diffusion in a singularly perturbed domain with a Robin-like boundary condition at each interface $\partial\mathcal{U}_j$. The main characteristic of a singularly perturbed domain is that the compartments $\mathcal{U}_j$ are small compared to the size of the domain Ω and are well separated from each other and $\partial\Omega$. More precisely, suppose that the domain Ω is inscribed by a rectangular area or volume whose smallest dimension is L, and introduce the dimensionless small parameter $\epsilon = r_{\max}/L$ with $0 < \epsilon \ll 1$ and $R_j(t) \leqslant r_{\max}$ for all $t \geqslant 0$ and $j = 1, \ldots, N$. We then fix the length scale by setting $L = 1$ and assume that $|\mathbf{x}_i - \mathbf{x}_j| = O(1)$ for all $j \neq i$ and $\min_{\mathbf{s}}\{|\mathbf{x}_j - \mathbf{s}|, \mathbf{s} \in \partial\Omega\} = O(1)$, $j = 1, \ldots, N$. One major difference between the two models is that Eq. (2.3) couples the interfacial particle flux to the growth of a cluster while Eq. (2.5) couples the flux to the intracellular reaction kinetics. In the QS model, asymptotic methods have been used to reduce the PDE-ODE system to an effective nonlinear ODE system in the well-mixed limit $D \gg O(\nu^{-1})$ with $\nu = -1/\ln\epsilon$ [13,14], and this analysis has subsequently been extended to the regime $D = O(\nu^{-1})$ [15]. The advantage of the latter regime is that it maintains the effects of weak diffusion-mediated interactions between clusters. In addition, extensive numerical simulations of the full model equations have established the accuracy of the asymptotic approximations for sufficiently small ν [14,15]. Here we apply the matched asymptotic methods of Ref. [15] to the cluster model given by Eqs. (2.2) and (2.3) to derive an $(N + 1)$-dimensional ODE system which couples the mean bulk protein concentration

$$\overline{c}(t) = \frac{1}{|\Omega\backslash\mathcal{U}(t)|}\int_{\Omega\backslash\mathcal{U}(t)} c(\mathbf{x}, t)d\mathbf{x} \tag{2.6}$$

to the cluster radii $R_j(t)$, $j = 1, \ldots, N$. We then use the reduced ODE model to explore the steady-state solutions and the rate of convergence to steady state for a range of geometric configurations.

III. ASYMPTOTIC REDUCTION TO A NONLINEAR ODE MODEL

The first step in the asymptotic reduction procedure is to integrate Eq. (2.2a) with respect to $\mathbf{x} \in \Omega\backslash\mathcal{U}$:

$$\frac{d\overline{c}(t)}{\partial t} + \gamma_0\overline{c}(\mathbf{x}, t) - I_0 = \frac{D}{|\Omega|}\int_{\Omega\backslash\mathcal{U}}\nabla^2 c(\mathbf{x}, t)d\mathbf{x}. \tag{3.1}$$

We have taken $|\Omega\backslash\mathcal{U}| = |\Omega| + o(\epsilon)$ on the left-hand side, which is valid provided N is not too large. The divergence theorem and the boundary conditions (2.2b) and (2.2c) imply that

$$\begin{aligned}\int_{\Omega\backslash\mathcal{U}}\nabla^2 c(\mathbf{x}, t)d\mathbf{x} &= \int_{\partial\Omega}\nabla c(\mathbf{x}, t)\cdot\mathbf{n}d\mathbf{x} \\ &\quad - \sum_{j=1}^{N}\int_{\partial\mathcal{U}_j}\nabla c(\mathbf{x}, t)\cdot\mathbf{n}_j d\mathbf{x} \\ &= -\frac{\kappa}{D}\int_{\partial\mathcal{U}_j} c(\mathbf{x}, t)d\mathbf{x}.\end{aligned} \tag{3.2}$$

To ensure that the particle flux across each cluster boundary $\partial\mathcal{U}_j$ is $O(1)$, we rescale the reactivity according to $\kappa = \kappa_0/\epsilon$. Combining Eqs. (3.1) and (3.2) then gives

$$\frac{d\overline{c}(t)}{\partial t} + \gamma_0\overline{c}(t) - I_0 = -\frac{1}{\epsilon|\Omega|}\sum_{j=1}^{N}\kappa_0\int_{\partial\mathcal{U}_j} c(\mathbf{x}, t)d\mathbf{x}. \tag{3.3}$$

We now construct an inner solution around each cluster. We introduce the stretched local variable $\mathbf{y} = \varepsilon^{-1}(\mathbf{x} - \mathbf{x}_j)$ and set

$C_j(\mathbf{y},t) = c(\mathbf{x}_j + \varepsilon\mathbf{y}, t)$. The inner equation for C_j then takes the form [after dropping the $O(\epsilon)$ time-derivative term]

$$D\nabla^2_{\mathbf{y}} C_j(\mathbf{y},t) = 0, \quad |\mathbf{y}| > \rho_j(t), \tag{3.4a}$$

$$\nabla_{\mathbf{y}} C_j(\mathbf{y},t)\cdot\mathbf{n}_j(\mathbf{y}) = \frac{\kappa_0}{D} C_j(\mathbf{y},t), \quad |\mathbf{y}| = \rho_j(t), \tag{3.4b}$$

where $R_j(t) = \epsilon\rho_j(t)$. Using polar coordinates with $|\mathbf{y}| = \rho$ and setting $C_j = C_j(\rho,t)$, we have the solution

$$C_j(\rho,t) = A_j(t)\left(\frac{D}{\kappa_0\rho_j(t)} + \log(\rho/\rho_j(t))\right) \tag{3.5}$$

for $\rho_j(t) \leqslant \rho < \infty$, where the amplitude $A_j(t)$ has yet to be determined. Substituting the inner solution into Eq. (3.3) using

$$\int_{\partial\mathcal{U}_j} c(\mathbf{x},t)d\mathbf{x} = 2\pi\epsilon\rho_j(t)C_j(\rho_j(t),t) = \frac{2\pi\epsilon A_j(t)D}{\kappa_0} \tag{3.6}$$

then gives

$$\frac{d\overline{c}(t)}{\partial t} + \gamma_0\overline{c}(t) - I_0 = -\frac{2\pi D}{|\Omega|}\sum_{j=1}^{N} A_j(t). \tag{3.7}$$

Similarly, substituting the inner solution into Eq. (2.3) and using the Robin boundary condition, we have

$$2\pi u_0'\rho_j(t)\frac{d}{dt}\rho_j(t) = 2\pi DA_j(t) - \gamma_0 u_0'\pi\rho_j^2(t). \tag{3.8}$$

It remains to determine the coefficients $A_j(t)$, $j = 1,\ldots,N$ by matching the inner solution with the outer solution. The latter satisfies the outer problem

$$\frac{\partial u(\mathbf{x},t)}{\partial t} = D\nabla^2 u(\mathbf{x},t) - \gamma_0 u(\mathbf{x},t) + I_0 \tag{3.9a}$$

for $\mathbf{x}\in\Omega\backslash\{\mathbf{x}_1,\ldots,\mathbf{x}_N\}$, with the boundary condition

$$D\nabla u(\mathbf{x},t)\cdot\mathbf{n}(\mathbf{x}) = 0, \ \mathbf{x}\in\partial\Omega, \tag{3.9b}$$

and the singularity conditions

$$u(\mathbf{x},t) \sim A_j(t)\log(|\mathbf{x}-\mathbf{x}_j|/\epsilon\rho_j(t)) + \frac{D}{\kappa_0\rho_j(t)}A_j(t) \tag{3.9c}$$

as $\mathbf{x}\to\mathbf{x}_j$.

To eliminate the $-\ln\epsilon = 1/\nu$ term in the singularity condition (3.9c), we rescale the unknown coefficients A_j by setting $A_j = \nu\mathcal{A}_j$. We also rescale the diffusivity by setting $D = D_0/\nu$ with $D_0 = O(1)$. This ensures that all terms in Eq. (3.7) are of the same order. We then set

$$u(\mathbf{x},t) = \overline{u}(t) + \nu u_1(\mathbf{x},t), \tag{3.10}$$

with $\int_\Omega u_1(\mathbf{x},t)d\mathbf{x} = 0$. Substituting into the outer equations shows that [15]

$$D_0\nabla^2 u_1(\mathbf{x},t) = \frac{d\overline{u}(t)}{dt} + \gamma_0\overline{u}(t) - I_0 + 2\pi D_0\sum_{k=1}^{N}\mathcal{A}_k(t)\delta(\mathbf{x}-\mathbf{x}_k), \tag{3.11a}$$

$$D\nabla u_1(\mathbf{x},t)\cdot\mathbf{n}(\mathbf{x}) = 0, \quad \mathbf{x}\in\partial\Omega, \tag{3.11b}$$

$$u_1(\mathbf{x},t) \sim -\frac{\overline{u}(t)}{\nu} + \mathcal{A}_j(t)\log(|\mathbf{x}-\mathbf{x}_j|/\rho_j(t)) + \left[1 + \frac{D_0}{\kappa_0\rho_j(t)}\right]\frac{\mathcal{A}_j(t)}{\nu}. \tag{3.11c}$$

The sum over the Dirac delta functions in Eq. (3.11) ensures consistency with Eq. (3.7) when integrated over Ω.

To incorporate the singularities, we expand u_1 as

$$u_1(\mathbf{x},t) \sim -2\pi D_0\sum_{k=1}^{N}\mathcal{A}_k(t)\mathcal{G}(\mathbf{x},\mathbf{x}_k), \tag{3.12}$$

where $\mathcal{G}$ is the Neumann Green's function

$$D_0\nabla^2\mathcal{G} = \frac{1}{|\Omega|} - \delta(\mathbf{x}-\mathbf{x}'), \quad \mathbf{x},\mathbf{x}'\in\Omega, \tag{3.13a}$$

$$\mathbf{n}\cdot\nabla\mathcal{G} = 0 \text{ on } \partial\Omega, \quad \int_\Omega \mathcal{G}d\mathbf{x} = 0. \tag{3.13b}$$

The additional constant term $1/|\Omega|$ on the right-hand side of Eq. (3.13a) is needed to ensure that both sides yield zero when integrating with respect to $\mathbf{x}\in\Omega$. The condition $\int_\Omega \mathcal{G}d\mathbf{x} = 0$ determines $\mathcal{G}$ uniquely. Note that the 2D Green's function can be decomposed as

$$\mathcal{G}(\mathbf{x},\mathbf{x}') = -\frac{\ln|\mathbf{x}-\mathbf{x}'|}{2\pi D_0} + \mathcal{R}(\mathbf{x},\mathbf{x}'), \tag{3.14}$$

where $\mathcal{R}$ is the regular part of $\mathcal{G}$. Finally, matching the inner and outer solutions using Eq. (3.11c) gives

$$\overline{c}(t) = \left[1 + \frac{D_0}{\kappa_0\rho_j(t)} - \nu\log\rho_j(t) + 2\pi\nu D_0\mathcal{R}(\mathbf{x}_j,\mathbf{x}_j)\right]\mathcal{A}_j(t) + 2\pi\nu D_0\sum_{k\neq j}^{N}\mathcal{G}(\mathbf{x}_j,\mathbf{x}_k)A_k(t). \tag{3.15}$$

It is convenient to rewrite (3.15) as the matrix equation

$$[\Gamma(t)\mathbf{I} + \nu\boldsymbol{\mathcal{M}}(t)]\boldsymbol{\mathcal{A}}(t) = \overline{c}(t)\mathbf{e}, \tag{3.16}$$

where $\mathbf{I}$ is a unit matrix, $\mathbf{e} = (1,1,\ldots,1)^\top$, $\boldsymbol{\mathcal{A}}(t) = (\mathcal{A}_1(t),\ldots,\mathcal{A}_N(t))^\top$, and

$$\mathcal{M}_{ij} = 2\pi D_0\mathcal{G}(\mathbf{x}_i,\mathbf{x}_j), \quad i\neq j, \tag{3.17a}$$

$$\mathcal{M}_{jj} = 2\pi D_0\mathcal{R}(\mathbf{x}_j,\mathbf{x}_j) - \log\rho_j(t), \tag{3.17b}$$

$$\Gamma(t) = 1 + \frac{D_0}{\kappa_0\rho_j(t)}. \tag{3.17c}$$

Only the diagonal terms of $\boldsymbol{\mathcal{M}}(t)$ are t dependent. Assuming that $\boldsymbol{\mathcal{M}}(t)$ is invertible (which certainly holds for sufficiently small ν), we set $DA_j(t) = D_0\mathcal{A}_j(t)$ in Eq. (3.7) to give

$$\frac{d\overline{c}(t)}{\partial t} + \gamma_0\overline{c}(t) - I_0 = -\frac{2\pi D_0\overline{c}(t)}{|\Omega|}\sum_{j,k=1}^{N}[\Gamma(t)\mathbf{I} + \nu\boldsymbol{\mathcal{M}}(t)]^{-1}_{jk}. \tag{3.18a}$$

Similarly, Eq. (3.8) becomes

$$\frac{d\rho_j(t)}{dt} = \frac{D_0\overline{c}(t)}{u_0'\rho_j(t)}\sum_{k=1}^{N}[\Gamma(t)\mathbf{I} + \nu\boldsymbol{\mathcal{M}}(t)]^{-1}_{jk} - \frac{\gamma_0}{2}\rho_j(t). \tag{3.18b}$$

Equations (3.18a) and (3.18b) are the main results of our asymptotic analysis. They form an $N+1$-dimensional system of ODEs that determines the cluster radii and mean bulk concentration. Setting time derivatives to zero in Eqs. (3.18a)

and (3.18b) yields the corresponding steady-state equations

$$\bar{c}^* = c_0\left(1 - \frac{2\pi D_0}{\gamma_0|\Omega|}\sum_{j,k=1}^{N}[\Gamma^*\mathbf{I} + \nu\boldsymbol{\mathcal{M}}^*]^{-1}_{jk}\right)^{-1} \tag{3.19a}$$

and

$$(\rho_j^*)^2 = \frac{2D_0\bar{c}^*}{\gamma_0 u_0'}\sum_{k=1}^{N}[\Gamma^*\mathbf{I} + \nu\boldsymbol{\mathcal{M}}^*]^{-1}_{jk}, \tag{3.19b}$$

with

$$\Gamma^* = 1 + \tfrac{D_0}{\kappa_0\rho_j^*}, \quad \mathcal{M}^*_{jj} = 2\pi D_0\mathcal{R}(\mathbf{x}_j, \mathbf{x}_j) - \log\rho_j^*. \tag{3.20}$$

A number of observations can be made:

(i) The right-hand sides of Eqs. (3.18a) and (3.18b) are nonperturbative functions of the small parameter ν. That is, the expressions effectively sum over all logarithmic terms, which is equivalent to calculating the asymptotic solution for all terms of $O(\nu^k)$ for any k. Obtaining a nonperturbative solution is important, since $\nu \to 0$ more slowly than $\epsilon \to 0$, and is a characteristic feature of diffusion problems in 2D singularly perturbed domains [21].

(ii) The cluster radii are coupled to each other and the bulk concentration nonlinearly even at $O(1)$ with respect to an asymptotic expansion in ν. In particular, Eqs. (3.18a) and (3.18b) become

$$\frac{d\bar{c}(t)}{\partial t} = -\gamma_0\bar{c}(t) + I_0 - \frac{2\pi D_0\bar{c}(t)}{|\Omega|}\sum_{j=1}^{N}\frac{\rho_j(t)}{\rho_j(t) + D_0/\kappa_0} \tag{3.21a}$$

and

$$\frac{d\rho_j(t)}{dt} = \frac{D_0\bar{c}(t)}{u_0'}\frac{1}{\rho_j(t) + D_0/\kappa_0} - \frac{\gamma_0}{2}\rho_j(t). \tag{3.21b}$$

(iii) The diffusion-mediated dependence on the geometry of the domain Ω and the positions of the anchoring sites $\mathbf{x}_j$ arises at $O(\nu)$. This information is contained with the Green's function terms.

(iv) $\bar{c}^* < c_0$ at $O(1)$.

IV. ANALYSIS OF THE REDUCED ODE SYSTEM

A. $O(1)$ planar dynamics

The existence of a stable multicluster state can be established from the $O(1)$ Eqs. (3.21a) and (3.21b). First note that if $\rho_j(0) = \rho_0$ for all $j = 1, \ldots, N$, then $\rho_j(t) = \rho(t)$ for all $j = 1, \ldots, N$ and $t > 0$. That is, $(\bar{c}(t), \rho(t))$ evolves on a two-dimensional invariant manifold for the dynamical system:

$$\begin{aligned}\frac{d\bar{c}(t)}{\partial t} &= F(\bar{c}(t), \rho(t)) \\ &\equiv -\gamma_0\bar{c}(t) + I_0 - \frac{2\pi N D_0\bar{c}(t)}{|\Omega|}\frac{\rho(t)}{\rho(t) + D_0/\kappa_0},\end{aligned} \tag{4.1a}$$

$$\begin{aligned}\frac{d\rho(t)}{dt} &= G(\bar{c}(t), \rho(t)) \\ &\equiv \frac{D_0\bar{c}(t)}{u_0'}\frac{1}{\rho(t) + D_0/\kappa_0} - \frac{\gamma_0}{2}\rho(t).\end{aligned} \tag{4.1b}$$

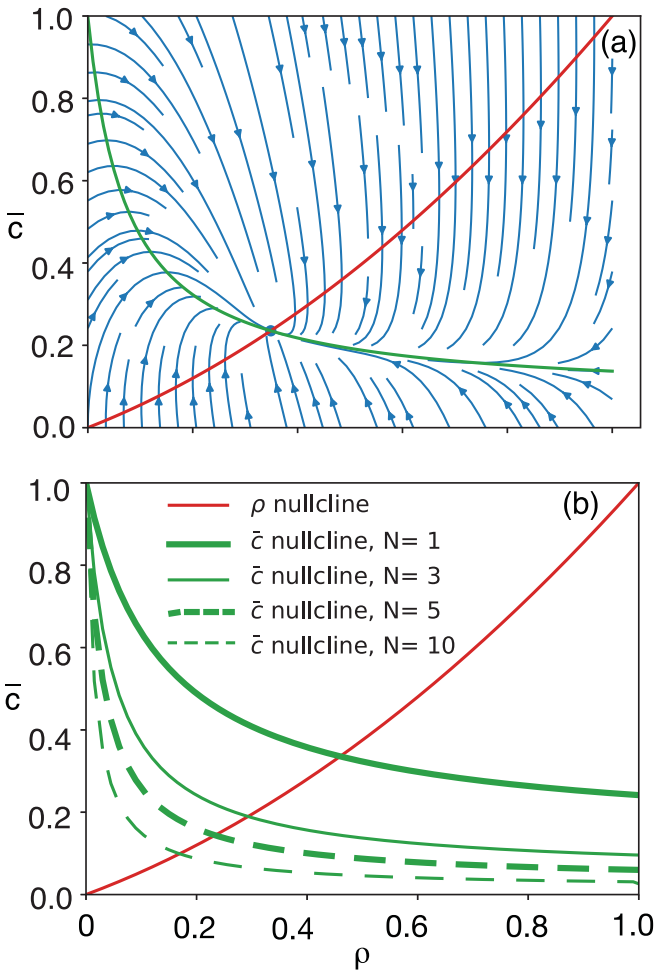

FIG. 3. (a) Phase flow and nullclines of the system (4.1a) and (4.1b) with the number of clusters $N = 2$. The other parameters, including D_0, κ_0, γ_0, I_0, u_0', $|\Omega|$, are all taken to be 1. (b) Nullclines for other N values.

The planar dynamical system can be analyzed by plotting the nullclines and phase flow as in Fig. 3(a). The nullcline $F(\bar{c}, \rho) = 0$ can be written in the form $\bar{c} = \bar{c}_1(\rho)$ with

$$\bar{c}_1(\rho) = I_0\left(\gamma_0 + \frac{2\pi N D_0}{|\Omega|}\frac{\rho}{\rho + D_0/\kappa_0}\right)^{-1}. \tag{4.2}$$

Note that $\bar{c}(\rho)$ is a positive, monotonically decreasing function of ρ with

$$\bar{c}_1(\rho) = 0, \quad \lim_{\rho\to\infty}\bar{c}_2(\rho) = I_0\left(\gamma_0 + \frac{2\pi N D_0}{|\Omega|}\right)^{-1}. \tag{4.3}$$

Similarly, the nullcline $G(\bar{c}, \rho) = 0$ can be written in the form $\bar{c} = \bar{c}_2(\rho)$ with

$$\bar{c}_2(\rho) = \frac{\gamma_0 u_0'}{2D_0}\rho\left(\rho + \frac{D_0}{\kappa_0}\right), \tag{4.4}$$

which is a monotonically increasing function of ρ with $\bar{c}_2(\rho) = 0$. Due to the monotonicity of the nullclines, there is a unique steady state $(\bar{c}^*, \rho^*)$ given by the intersection of the two nullclines. The phase flow establishes that the fixed point is stable with respect to perturbations restricted to the invariant

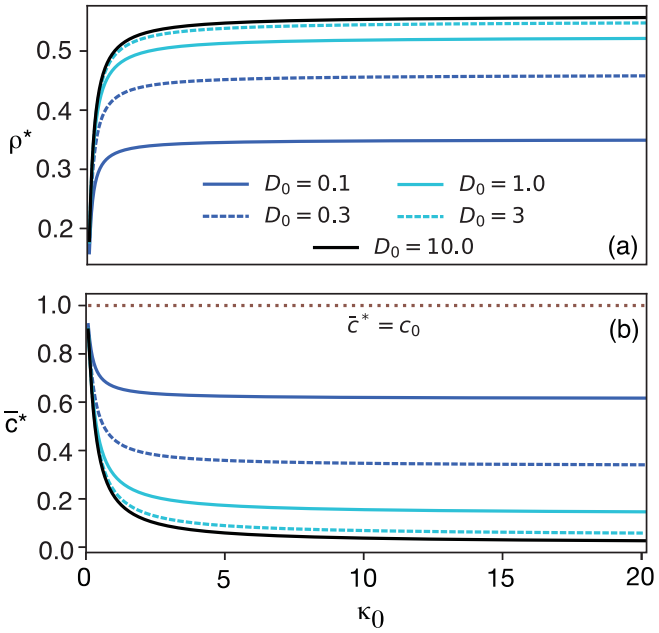

FIG. 4. Leading order steady-state values for various values of κ_0, D_0. The system is normalized such that $\gamma_0 = |\Omega| = u_0' = c_0 = 1$ and $N = 4$. The dotted line in the lower graph is the equilibrium concentration when no clusters are present, with $\bar{c}^* = c_0$.

manifold. The shift in the steady state with N is illustrated in Fig. 3(b).

Figure 4 depicts how the steady state depends on the values of (κ_0, D_0). We notice that as κ_0 increases, the steady state rapidly converges to the totally absorbing limit ($\kappa_0 \to \infty$), while increments in D_0 have diminishing returns for $D_0 = O(1)$. For the sake of illustration, we take the number of clusters to be $N = 4$. The graphs for other values of N follow similar patterns. Even for a single cluster, the steady state value of $\bar{c}^*$ differs significantly from the no-clusters-equilibrium concentration c_0 when $\kappa_0, D_0 = O(1)$. This is, as expected, due to the well-mixed limit amplifying the influence of clusters to a global range. Indeed, we find from Eqs. (3.19a) and (3.19b) that

$$\bar{c}^* = c_0 - \frac{\pi u_0' N}{|\Omega|}\rho^{*2}, \tag{4.5}$$

which suggests a form of conservation law. The total number of particles in the entire domain Ω is independent of the number of clusters in the domain. The mean concentration in the bulk domain adjusts to compensate for the extra clusters so the total number of particles is that of a domain without clusters and balanced only by recycling and reinsertion.

B. Linear stability analysis of the full system

Since the unique fixed point of the full dynamical system (3.18a) and (3.18b) is hyperbolic, its stability for sufficiently small ν can be determined by the stability at $O(1)$, since the higher order terms only contribute $O(\nu)$ to the eigenvalues and modes. Combining Eqs. (3.18a) and (3.18b) and linearizing the system around the steady state $(\bar{c}^*, \rho^*)$, the full $N+1$-dimensional system at $O(1)$ is of the form

$$\dot{\mathbf{v}} = \mathcal{N}\mathbf{v}, \tag{4.6}$$

with $\mathbf{v} = (\delta\bar{c}(t), \delta\boldsymbol{\rho}(t))^\top$. Note that all $\mathcal{N}_{1i}$ are equal for $i > 1$, and similarly for all $\mathcal{N}_{i1}$'s and $\mathcal{N}_{ii}$'s, due to the symmetry imposed on the clusters. All nonzero entries of matrix $\mathcal{N}$ therefore equals to one of four common values:

$$\mathcal{N}_{11} = \mathcal{K}_1 := -\left(D_0 \frac{2\pi N}{|\Omega|}\frac{1}{1+\frac{D_0}{\kappa_0\rho^*}} + \gamma_0\right), \tag{4.7a}$$

$$\mathcal{N}_{1i} = \mathcal{K}_2 := -\left(\frac{D_0^2}{\kappa_0}\frac{2\pi}{|\Omega|}\frac{1}{\left(\rho^* + \frac{D_0}{\kappa_0}\right)^2}\right)\bar{c}^*, \quad i \neq 1, \tag{4.7b}$$

$$\mathcal{N}_{i1} = \mathcal{K}_3 := \frac{D_0}{u_0'}\frac{1}{\rho^* + \frac{D_0}{\kappa_0}}, \quad i \neq 1, \tag{4.7c}$$

$$\mathcal{N}_{ii} = \mathcal{K}_4 := -\frac{D_0}{u_0'}\frac{\bar{c}^*}{\left(\rho^* + \frac{D_0}{\kappa_0}\right)^2} - \frac{\gamma_0}{2}. \quad i \neq 1, \tag{4.7d}$$

with $(\bar{c}^*, \boldsymbol{\rho}^*)$ the steady state solution. For compact presentation, we will use $i = 2$ to represent these common values.

By calculating the determinant using the first row of $\mathcal{N} - \lambda I$, one can show that

$$\det(\mathcal{N} - \lambda I) = (\mathcal{K}_1 - \lambda)(\mathcal{K}_4 - \lambda)^N - N\mathcal{K}_2\mathcal{K}_3(\mathcal{K}_4 - \lambda)^{N-1}, \tag{4.8}$$

where I is the $N+1$ dimensional identity matrix. The planar dynamical system is recovered by setting $N = 1$ for which the Jacobian has the two roots

$$\lambda_\pm = \frac{\mathcal{K}_1 + \mathcal{K}_4 \pm \sqrt{(\mathcal{K}_1 - \mathcal{K}_4)^2 + 4N\mathcal{K}_2\mathcal{K}_3}}{2}. \tag{4.9}$$

On the other hand, for $N > 1$ we have the additional eigenvalue

$$\lambda = \mathcal{K}_4 < 0, \tag{4.10}$$

with multiplicity $N - 1$. This eigenvalue determines the rate of convergence to the invariant manifold. Since $\mathcal{K}_1, \mathcal{K}_4 < 0$, it follows that the system is unstable if and only if

$$N\mathcal{K}_2\mathcal{K}_3 > \mathcal{K}_1\mathcal{K}_4. \tag{4.11}$$

We find that

$$\mathcal{K}_2\mathcal{K}_3 = -\left(\frac{D_0^3}{\kappa_0 u_0'}\frac{2\pi}{|\Omega|}\frac{1}{\left(\rho^* + \frac{D_0}{\kappa_0}\right)^3}\right)\bar{c}^* < 0, \tag{4.12}$$

$$\mathcal{K}_1\mathcal{K}_4 = \left(D_0\frac{2\pi N}{|\Omega|}\frac{1}{1+\frac{D_0}{\kappa_0\rho^*}} + \gamma_0\right) \times \left(\frac{D_0}{u_0'}\frac{\bar{c}^*}{\left(\rho^* + \frac{D_0}{\kappa_0}\right)^2} + \frac{\gamma_0}{2}\right) > 0, \tag{4.13}$$

so the system is always stable.

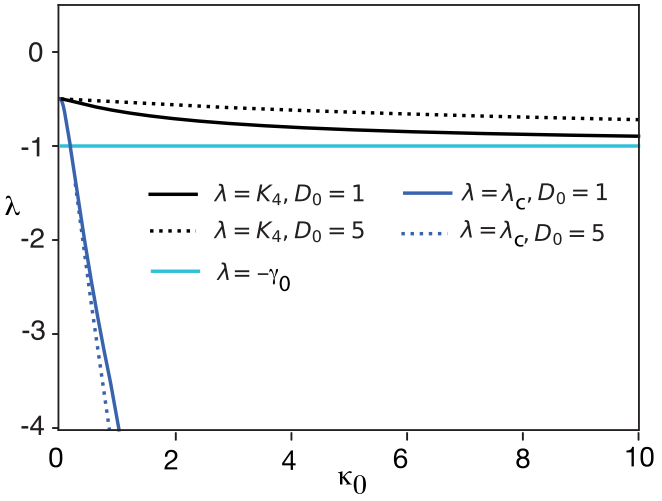

FIG. 5. Plots of the eigenvalues $\lambda = \mathcal{K}_4$, $\lambda = -\gamma_0$, and λ_c for a range of κ_0 and $D_0 = 1, 5$, respectively. Here $\gamma_0 = u_0' = c_0 = |\Omega| = 1$ and $N = 2$. For both values of D_0, the $\mathcal{K}_4$ eigenvalue is the largest and converges to $-\gamma_0$. The convergence is slower if D_0 is large.

After some algebra, it can be shown that one of the two eigenvalues $\lambda_\pm$ is $-\gamma_0$. Using the conservation of trace when diagonalizing $\mathcal{N}$, we find that the other eigenvalue of the pair, which we denote by λ_c, satisfies

$$\lambda_c - \gamma_0 + (N-1)\mathcal{K}_4 = tr(\mathcal{N}) = \mathcal{K}_1 + N\mathcal{K}_4,$$
$$\Rightarrow \lambda_c = \mathcal{K}_1 + \mathcal{K}_4 + \gamma_0. \tag{4.14}$$

Since $\mathcal{K}_1 < -\gamma_0 < 0$, it can also be shown that $-\gamma_0 < \mathcal{K}_4 < -\gamma_0/2 < 0$. Therefore, the mode corresponding to eigenvalue $\lambda = \mathcal{K}_4$ dominates as $t \to \infty$. This ordering of the eigenvalues can also be observed in Fig. 5. In the totally absorbing limit $\kappa_i \to \infty, i = 1, 2, \ldots, N$, the rates of decay to steady state for the clusters all converges to $-\gamma_0$ in general, however, this convergence is much slower for larger values of D_0, requiring a much larger change in κ_0 for a diminishing change in the largest rate. In the reflecting boundary limit $\kappa_i \to 0$ on the other hand, the convergence rates all approach $-\gamma_0/2$, which corresponds to the natural shrink rate of a two-dimensional cluster from recycling alone. Finally, in Fig. 6 we show sample trajectories for N clusters with $\rho_j(0) = \rho_c$ for $j = 1, \ldots, N-1$ and $\rho_N(0) = \rho_d \neq \rho_c$. Convergence to the invariant manifold $(\rho_c, \bar{c})$ can clearly be seen.

V. PAIR OF CLUSTERS IN THE UNIT DISC

The dependence on the steady-state cluster sizes on the geometry of the domain arises at $O(\nu)$. Here we illustrate this by considering the example of two clusters in the unit disk as shown in Fig. 7. The two clusters $\mathcal{U}_i$ of radii $R_i(t) = \epsilon\rho_i(t), i = 1, 2$ are centered at $\mathbf{x}_1, \mathbf{x}_2$. Due to the rotational symmetry of the domain, without loss of generality one may take the first cluster to be centered on the positive x axis.

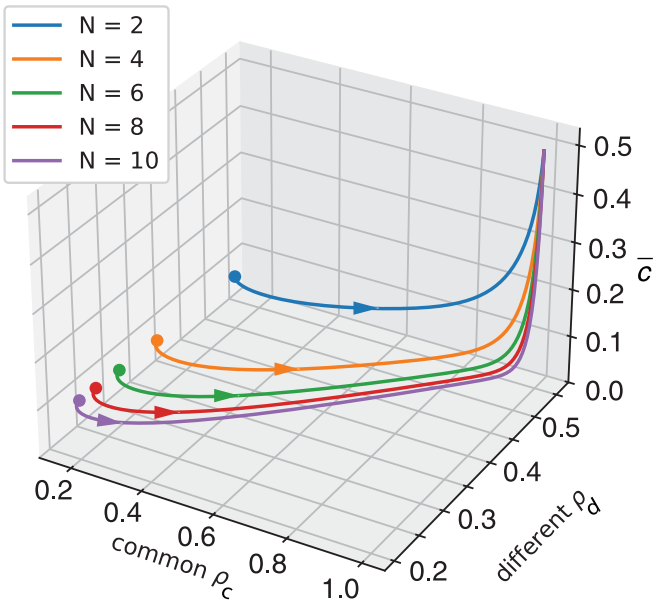

FIG. 6. Example trajectories for N clusters with $\rho_j(0) = \rho_c$ for $j = 1, \ldots, N-1$ and $\rho_N(0) = \rho_d \neq \rho_c$. All other parameters are taken to be 1.

Therefore, the configuration of the system is as follows:

$$|\Omega| = 2\pi,\ \mathbf{x}_1 = a\mathbf{e}_1,\ \mathbf{x}_2 = b\mathbf{e}_1,\ 0 \leqslant a < 1, \quad 0 < b < 1. \tag{5.1}$$

Here $\mathbf{e}_1 = (1, 0)^\top$, and $\mathbf{e}$ is a general unit vector that makes an angle $\theta \in [0, \pi]$ with $\mathbf{e}_1$, such that $\mathbf{e} \cdot \mathbf{e}_1 = \cos\theta$. The Green's function on this domain is known explicitly to be [21]

$$G_0(\mathbf{x}, \xi) = \frac{1}{2\pi}\left[-\ln(|\mathbf{x} - \xi|) - \ln\left(\left|\mathbf{x}|\xi| - \frac{\xi}{|\xi|}\right|\right) + \frac{1}{2}(|\mathbf{x}|^2 + |\xi|^2) - \frac{3}{4}\right]. \tag{5.2}$$

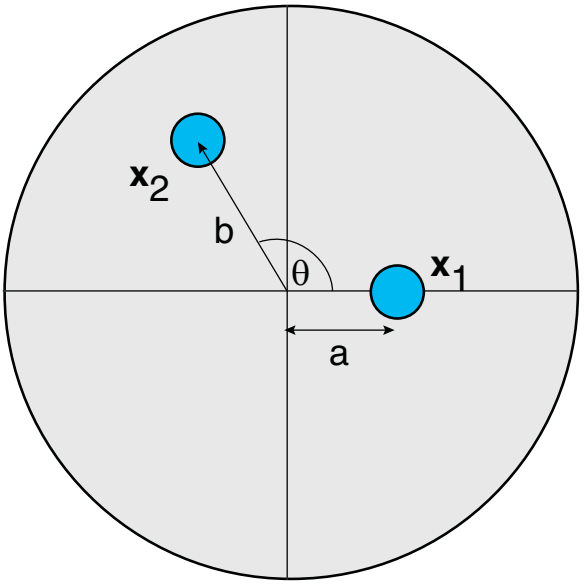

FIG. 7. Pair of clusters in the unit disk.

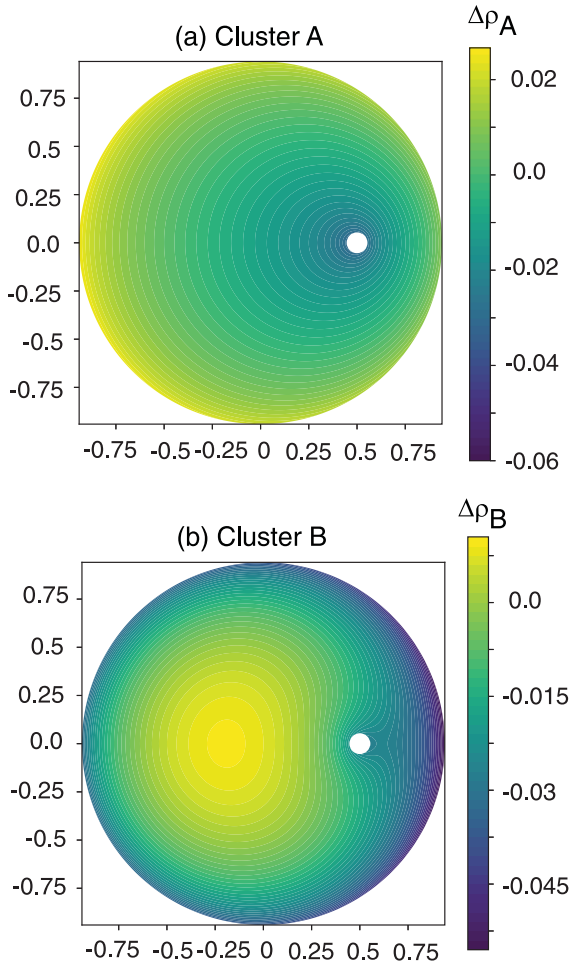

FIG. 8. Effect of ν-dependent corrections of the steady state radii for two clusters A and B in the unit disk, see Fig. 6, with cluster A fixed at (0.5,0) and $\nu = 0.2$. (a) First-order correction $\Delta\rho_A$ to the radius of cluster A as the position of cluster B is varied in the unit disk. (b) Corresponding first-order correction $\Delta\rho_B$ to the radius of cluster B. In both figures, leading order equilibrium values are $\rho_A^*(0) = \rho_B^*(0) \approx 0.54$. To maintain the well-separated assumption imposed on clusters A, B, and the boundary $\partial\Omega$, we take the radial position of cluster B to satisfy $0 < b < 0.95$ while the centers satisfy $|\mathbf{x}_1 - \mathbf{x}_2| > 0.05$, see Eqs. (5.1). Other parameters are $D_0 = \gamma_0 = u_0' = \kappa_0 = I_0 = 1$.

For the given configuration, we thus have

$$\begin{aligned}\mathcal{G}(\mathbf{x}_1,\mathbf{x}_2) &= \frac{1}{2\pi}\Big[-\ln(|b\mathbf{e}-a\mathbf{e}_1|)\\ &\quad -\ln(|ab\mathbf{e}_1-\mathbf{e}|)+\frac{1}{2}(a^2+b^2)-\frac{3}{4}\Big],\\ &= \frac{1}{2\pi}\Big[-\frac{1}{2}\ln(a^2+b^2-2ab\cos\theta)\\ &\quad -\frac{1}{2}\ln(a^2b^2+1-2ab\cos\theta)\\ &\quad +\frac{1}{2}(a^2+b^2)-\frac{3}{4}\Big], \end{aligned} \tag{5.3a}$$

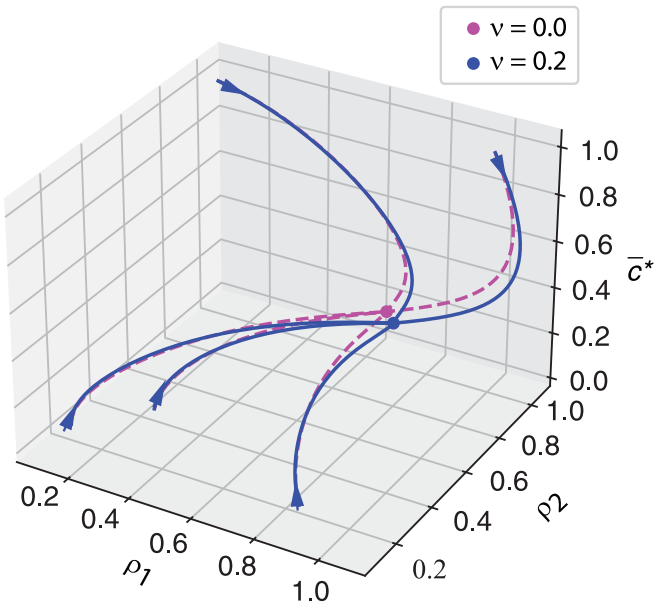

FIG. 9. Example trajectories for a pair of clusters. Here $a = 0.4$, $b = 0.8$, $\theta = 2$, $\kappa_0 = 5$ for all contours, and $|\Omega| = \pi$. Other parameters are as in Fig. 8. The dynamics is largely the same, besides a small shift in the steady state.

and

$$\mathcal{R}(\mathbf{x}_1,\mathbf{x}_1) = \frac{1}{2\pi}\Big[-\ln(1-a^2)+a^2-\frac{3}{4}\Big], \tag{5.3b}$$

$$\mathcal{R}(\mathbf{x}_2,\mathbf{x}_2) = \frac{1}{2\pi}\Big[-\ln(1-b^2)+b^2-\frac{3}{4}\Big]. \tag{5.3c}$$

Let $\bar{c}^*(\nu)$ and $\rho_j^*(\nu)$ denote the solution of the steady-state Eqs. (3.19a) and (3.19b) for $N = 2$ and a given ν. The contour plots in Fig. 8 depict the ν-dependent corrections $\Delta\rho_j^*(\nu) = \rho_j^*(\nu) - \rho_j^*(0)$ for the two clusters as the position of the second cluster varies in the unit disk. Figure 9 shows example trajectories based on numerical simulations of Eqs. (3.18a) and (3.18b) for $\nu = 0$ and $\nu = 0.2$. Although there is a shift in the steady state, the qualitative behavior is largely the same. Finally, note that we could also consider other geometric configurations Ω such as the square, but extracting the regular part of the Green's function is considerably more involved [21].

VI. DISCUSSION

In this paper, we analyzed the existence and stability of the nonequilibrium stationary state of a protein aggregation model in the fast diffusion limit. Using matched asymptotic methods, we reduced the PDE model with moving interior boundaries to a nonlinear ODE system coupling the mean bulk concentration to the cluster radii. We thus established the existence and stability of a multicluster stationary state that is, at leading order, independent of the shape of the domain and the location of the clusters. Although we restricted our analysis to the regime $D = O(1/\nu)$, numerical simulations have previously shown that such a nonequilibrium stationary state persists for $D = O(1)$ [6]. Our asymptotic analysis thus

provides further support to the experimentally-motivated hypothesis [9] that the recycling of proteins between the surface and interior of a neuron combined with protein aggregation is a viable nonequilibrium mechanism for the formation of multiple postsynaptic domains.

One major simplification of the current model was to assume that the proteins within a cluster efficiently rearrange themselves to maintain a uniform concentration and a stable circular shape (in 2D). This allowed us to neglect the protein dynamics within a cluster and express the growth in terms of the cluster size. It would be interesting to develop a model that explicitly takes into account the dynamical rearrangement of proteins under the combined effects of aggregation at the cluster interface and recycling within the cluster interior. Such a model could be used to explore whether the resulting dynamics induces surface instabilities that break the circular symmetry of a cluster interface analogous to diffusion-limited-aggregation (DLA) in the absence of recycling and particle rearrangements [22,23].

Finally, from a more general perspective, both the protein-aggregation model, Eqs. (2.2) and (2.3), and the QS model, Eqs. (2.4) and (2.5), are examples of singularly perturbed diffusion problems in which interfacial diffusive fluxes drive nonlinear processes corresponding, respectively, to the growth of protein clusters and signal transduction networks within the interiors of bacterial cells. As shown here and in Refs. [13–15], matched asymptotic methods involving the small parameter $\nu = -1/\ln\epsilon$, where ϵ specifies the relative size of the clusters or cells within the bulk domain, can be used to reduce the hybrid PDE-ODE models to finite-dimensional ODE systems that are much simpler to analyze. In the case of cluster growth, the $O(1)$ terms are sufficient to establish the existence and stability of a multicluster stationary state. On the other hand, in the QS case, higher-order terms play a critical role in generating diffusion-induced synchronized oscillations across the population of cells [13–15].

DATA AVAILABILITY

There are no publicly available research data or software supporting this manuscript. Requests for further information or data should be sent to the authors.

[1] A. J. Borgdorff and D. Choquet, Regulation of AMPA receptor lateral movements, Nature (London) **417**, 649 (2002).

[2] D. Choquet, Linking nanoscale dynamics of AMPA receptor organization to plasticity of excitatory synapses and learning, J. Neurosci. **38**, 9318 (2018).

[3] M. Dahan, S. Levi, C. Luccardini, P. Rostaing, B. Riveau, and A. Triller, Diffusion dynamics of glycine receptors revealed by single-quantum dot tracking, Science **302**, 442 (2003).

[4] S. A. Maynard, J. Ranft, and A. Triller, Quantifying postsynaptic receptor dynamics: Insights into synaptic function, Nat. Rev. Neurosci. **24**, 4 (2023).

[5] J. Meier, C. Vannier, A. Serge, A. Triller, and D. Choquet, Fast and reversible trapping of surface glycine receptors by gephyrin, Nat. Neurosci. **4**, 253 (2001).

[6] R. Baillou and J. Ranft, Nonequilibrium cluster-cluster aggregation in the presence of anchoring sites, Phys. Rev. E **110**, 034410 (2024).

[7] P. C. Bressloff, Asymptotic analysis of particle cluster formation in the presence of anchoring sites, Eur. Phys. J. E **47**, 30 (2024).

[8] V. Hakim and J. Ranft, Lifetime of a structure evolving by cluster aggregation and particle loss, and application to postsynaptic scaffold domains, Phys. Rev. E **101**, 012411 (2020).

[9] J. Ranft, L. G. Almeida, P. C. Rodriguez, A. Triller, and V. Hakim, An aggregation-removal model for the formation and size determination of postsynaptic scaffold domains, PLoS Comput. Biol. **13**, e1005516 (2017).

[10] K. Chen and P. C. Bressloff, Protein cluster formation as a moving boundary problem (unpublished).

[11] D. R. Mclean and B. P. Graham, Mathematical formulation and analysis of a continuum model for tubulin-driven neurite elongation, Proc. R. Soc. London A **460**, 2437 (2004).

[12] D. R. Mclean and B. P .Graham, Stability in a mathematical model of neurite elongation, IMA Math. Med. Biol. **23**, 101 (2006).

[13] J. Gou and M. J. Ward, Asymptotic analysis of a 2-D model of dynamically active compartments coupled by bulk diffusion, J. Nonlinear Sci. **26**, 979 (2016).

[14] S. Iyaniwura and M. J. Ward, Localized signaling compartments in 2-D coupled by a bulk diffusion field: Quorum sensing and synchronous oscillations in the well-mixed limit, Eur. J. Appl. Math. **32**, 1001 (2021).

[15] S. Iyaniwura and M. J. Ward, Synchrony and oscillatory dynamics for a 2-D PDE-ODE model of diffusion-mediated communication between small signaling compartments, SIAM J. Appl. Dyn. Syst. **20**, 438 (2021).

[16] C. P. Brangwynne, P. Tompa, and R. V. Pappu, Polymer physics of intracellular phase transitions, Nat. Phys. **11**, 899 (2015).

[17] A. A. Hyman, C. A. Weber, and F. Julicher, Liquid-liquid phase separation in biology, Annu. Rev. Cell Dev. Biol. **30**, 39 (2014).

[18] M. Zeng, Y. Shang, Y. Arak, T. Guo, R. L. Huganir, and M. Zhang, Phase transition in postsynaptic densities underlies formation of synaptic complexes and synaptic plasticity, Cell **166**, 1163 (2016).

[19] D. Zwicker, A. A. Hyman, and F. Jülicher, Suppression of Ostwald ripening in active emulsions, Phys. Rev. E **92**, 012317 (2015).

[20] C. A. Weber, D. Zwicker, F. Jülicher, and C. F. Lee, Physics of active emulsions, Rep. Prog. Phys. **82**, 064601 (2019).

[21] M. J. Ward and J. B. Keller, Strong localized perturbations of eigenvalue problems, SIAM J. Appl. Math. **53**, 770 (1993).

[22] D. A. Kessler, J. Koplik, and H. Levine, Pattern selection in fingered growth phenomena, Adv. Phys. **37**, 255 (1988).

[23] T. A. Witten and L. M. Sander, Diffusion-limited aggregation, a kinetic critical phenomenon, Phys. Rev. Lett. **47**, 1400 (1981).